UNIVERSITY OF WEST LONDON
The Career University

UWL REPOSITORY

repository.uwl.ac.uk

Steel reinforced self-compacting concrete (SCC) cantilever beams: bond behaviour in poor condition zones

Montaser, Wael, Shaaban, Ibrahim ORCID logoORCID: https://orcid.org/0000-0003-4051-341X, Rizzuto, Joseph, Zaher, Amr, Rashad, Ahmed and El Sadany, Shorouk (2023) Steel reinforced self-compacting concrete (SCC) cantilever beams: bond behaviour in poor condition zones. International Journal of Concrete Structures and Materials. ISSN 1976-0485

http://dx.doi.org/10.1186/s40069-023-00581-9

This is the Published Version of the final output.

UWL repository link: https://repository.uwl.ac.uk/id/eprint/9725/

Alternative formats: If you require this document in an alternative format, please contact: open.research@uwl.ac.uk

Copyright: Creative Commons: Attribution 4.0

Copyright and moral rights for the publications made accessible in the public portal are retained by the authors and/or other copyright owners and it is a condition of accessing publications that users recognise and abide by the legal requirements associated with these rights.

Take down policy: If you believe that this document breaches copyright, please contact us at open.research@uwl.ac.uk providing details, and we will remove access to the work immediately and investigate your claim.

Rights Retention Statement:

International Journal of Concrete Structures and Materials

RESEARCH Open Access

Steel Reinforced Self-Compacting Concrete (SCC) Cantilever Beams: Bond Behaviour in Poor Condition Zones

Wael Mohamed Montaser[1*], Ibrahim Galal Shaaban[2], Joseph P. Rizzuto[2], Amr Hussein Zaher[3], Ahmed Rashad[3] and Shorouk Mohamed El Sadany[1]

Abstract

Previous investigations carried out on reinforced self-compacted concrete (SCC) beams have reported contradictory results on reinforcement bond behaviour occurring in the zones defined for good bond conditions according to Eurocode2. Cantilevered SCC beams' critical upper tension reinforcement bond behaviour has previously had limited reporting. In this study, the bond behaviour in normally vibrated concrete (NVC) and self-compacted concrete (SCC) in poor conditions zones are compared and the differences are highlighted. The effect of four parameters, including (i) concrete type (SCC and NVC), (ii) characteristic strength of SCC, (iii) lap splice length, and (iv) depth of concrete cover for the reinforcement is investigated. It was found that for the studied beams, increasing splice length improved the energy absorption and changed the failure mode to a more ductile manner even at the poor bond conditions zones. The maximum measured steel strains in SCC beams in the lap splice zones, were higher than those for NVC specimens. The mean bond stress values, for SCC beams with 25–50% lap splice lengths, were higher than those of NVC beams, with the same lap splice lengths, by 16–13%, respectively. The results of the current study showed that the empirical equations from the literature overestimated the bond strength of the splice lap length for cantilever upper steel in SCC beams with long splices which agrees with the state of the art as these equations were developed originally for short anchorage lengths.

Keywords Self-compacting concrete, Bond strength, Bond stress, Lap length of steel bars in tension, Empirical equations, Concrete cover, Poor bond conditions

1 Introduction

The use of self-compacting concrete (SCC) has been rapidly increasing for the past three decades. SCC is now widely used in many types of structures. A notable example of SCC use is in the anchorage blocks of the Akashi Kaikyo suspension bridge which opened in 1998 (Furuya et al., 1994).

The bond between concrete and reinforcing bars in splices is an essential requirement in the design of reinforced concrete (RC) structures Schiessl & Zilch, 2001). This has an important effect on the behaviour of reinforced concrete elements during the cracked stage (Schiessl & Zilch, 2001). Deflections are influenced by the bond stress distribution along the reinforcement bars and

Journal information: ISSN 1976-0485 / eISSN 2234-1315

*Correspondence:
Wael Mohamed Montaser
wmontaser.eng@o6u.edu.eg
[1] Construction and Building Department, Faculty of Engineering, October 6 University, Giza, Egypt
[2] School of Computing and Engineering, University of West London, St Mary's Road, Ealing W5 5RF, London, UK
[3] Structural Engineering Department, Faculty of Engineering, Ain Shams University, Cairo, Egypt

Springer Open

© The Author(s) 2023. **Open Access** This article is licensed under a Creative Commons Attribution 4.0 International License, which permits use, sharing, adaptation, distribution and reproduction in any medium or format, as long as you give appropriate credit to the original author(s) and the source, provide a link to the Creative Commons licence, and indicate if changes were made. The images or other third party material in this article are included in the article's Creative Commons licence, unless indicated otherwise in a credit line to the material. If material is not included in the article's Creative Commons licence and your intended use is not permitted by statutory regulation or exceeds the permitted use, you will need to obtain permission directly from the copyright holder. To view a copy of this licence, visit http://creativecommons.org/licenses/by/4.0/.

by the slippage between the bars and the surrounding concrete Domone, 2007). Various studies have been conducted on SCC bonding (Chan et al., 2003 The outcomes of these studies appear contradictory. Some researchers indicate that the bond stress between reinforcing steel bars and SCC are higher than that between reinforcing bars and normally vibrated concrete (NVC) (Pandurangan et al., 2010, Castel et al., 2006, Cattaneo and Rosati 2009). Others have reported either no differences between these types of concrete or lower bond stresses with SCC (Nepomuceno and Bernardo 2019, Esfahani et al. 2008, Ponmalar 2018, Khan and Ayub 2021). The European Guidelines for self-compacting concrete (Self-Compacting Concrete European Project Group, 2005) represents a state-of-the-art report used by designers, purchasers, specifiers, producers and other stake holders.

2 Literature Review

Chan et al. (Chan et al., 2003) studied the bond between concrete and steel reinforcements for SCC and ordinary concrete. Their results showed that SCC members had higher reinforcing bar bond than those exhibited in ordinary concrete. It was also found that the reduction in bond due to bleeding and heterogeneous nature, in the case of ordinary concrete, did not take place with SCC.

Pandurangan et al. (2010) tested beam specimens of dimensions (200 mm wide × 250 mm deep × 2200 mm long) to study the effect of using SCC on the bond strength and mode of bond failure of tension lap splices anchored in NVC. Each beam was arranged with spliced bars in a region at mid-span, where constant moment occurred and various levels of stirrup confinement were in place (Pandurangan et al., 2010). They agreed with Chan et al. (Chan et al., 2003) that there was an increase in the bond strength when SCC was used. They found also that ductility and splice strength increased as the confinement increase. In addition, the failure in the splice region took place as a result of yielding of the steel when the stirrup spacing was less than 150 mm (Pandurangan et al., 2010).

Kaihua Liu et al. (Liu et al., 2020) investigated the bond behaviour of deformed steel bars in SCC and NVC. Thirty-three cube specimens (with 150 mm sides and embedded steel bars) with different concrete compressive strengths, different concrete cover sizes of (2 d_b, 3 d_b, 4.2 d_b, and 5 d_b), and embedded lengths (3 d_b, 4 d_b, 5 d_b, and 6 d_b) were prepared and tested under pull-out loading. They found that the bond strength between reinforcing bars and SCC increased with increasing concrete strengths and concrete cover depth (Liu et al., 2020). Specimens with shorter embedded length showed higher bond strength (Liu et al., 2020). They concluded that deeper concrete covers and an increase in the transverse reinforcement can provide effective restraint and changes to the failure pattern from splitting failure to pull-out failure (Liu et al., 2020). They also found that the existing empirical and code models in the literature for bond strength prediction in NVC were all conservative and could be extended to SCC (Liu et al., 2020).

Turk et al. (Turk et al., 2008) tested twelve beam specimens of (2000 mm long × 300 mm deep × 200 mm wide) in bending to study the effect of SCC and the diameter of reinforcement on bond-slip of tension lap-splices. Test variables were concrete type (SCC and NVC) and reinforcing bar size (16 mm and 20 mm) (Turk et al., 2008). They found that increasing the diameter of the steel bar from 16 to 20 mm decreases the bond strength, and the normalised bond strengths of the SCC mixes were higher than those of the NC mixes by 4% only (Turk et al., 2008).

El-Azab et al. (El-Azab et al., 2014) tested sixteen simply supported beams. These were divided into four groups. All beams were of (1800 mm span and 200 mm wide × 400 mm deep) cross-sectional cast with high strength self-consolidated concrete (HSSCC) (El-Azab et al., 2014). Twelve beams contained splice-laps and these were located in the constant moment zone. Four beams without splices were used as control beams (El-Azab et al., 2014). Their results showed that the splice length of 40 bar diameters was the minimum to be taken as a sufficient splice length, as the beams started to show signs of cracking and failed at a load equal to or higher than those without splices (El-Azab et al., 2014). In addition, it was found that using a larger number of steel bars with smaller bar diameter increased both the beam ultimate capacity and ductility (El-Azab et al., 2014).

Wu et al. (Wu et al., 2018) investigated the lap splice bond strength in tension in NVC and SCC beams. Six beam specimens were cast and subjected to bending. They stated that the SCC and NVC beams presented similar bond strengths. In addition, both SCC and NVC beams with transverse stirrups had ductile flexural behaviour in the area of tension laps (Wu et al., 2018). They observed minor spalling between reinforcing steel and concrete under service loading (Wu et al., 2018).

Almeida et al. (Almeida Filho et al., 2008) studied the mechanical properties (compressive strength, modulus of elasticity and tensile strength) and bond strength of SCC by testing concrete cylinders (150 mm dia. × 300 mm deep) of 50 N/mm^2 compressive strength at 28 days. The studied variables were: (i) maximum aggregate size and (ii) SCC fluidity (concrete of very high workability using superplasticizer) (Almeida Filho et al., 2008). They concluded that the variability of the SCC was small for the modulus of elasticity and for the compressive strength,

but the tensile strength presented a significant variability due to the failure mode (Almeida Filho et al., 2008). In addition, the variability of the bond strength was small which indicated the reliability of SCC in the civil construction (Almeida Filho et al., 2008).

Zuo et al. (Zuo & Darwin, 2000) experimentally tested 64 specimens to study the effects of concrete properties on the splice strength of high relative strengths, ranging from 29 to 108 N/mm^2. They found that concrete containing stronger coarse aggregate had higher splice strength under different confinement conditions (Zuo & Darwin, 2000). In addition, for splices confined by transverse reinforcement, the contribution of transverse reinforcement to splice strength increased with the increase of coarse aggregate content in concrete (Zuo & Darwin, 2000). Moreover, the splice strength of bars confined by transverse reinforcement increased, with an increase in relative rib area and bar diameter (Zuo & Darwin, 2000).

Zhao et al. (Zhao et al., 2021) investigated bond behaviorus of FRP bars in ECC experimentally and numerically. A simplified bond failure model was established based on the pullout failure mode. Results indicated that increasing the ECC strength led to a proportional increase in the bond strength and rebars with higher ribs exhibited higher bond strengths (by a maximum of 55%) than counterparts with lower ribs.

Zhao et al. (Zhao et al., 2020) Studied the mechanical properties of steel–FRP composite SFCBs bars under tensile tests. Bond performance of SFCBs in concrete were tested. Results showed that SFCBs had bond strengths between round and ribbed rebars and the rebar diameter and surface treatment are key factors influencing the bond strength of SFCB–concrete interface (Zhao et al., 2020). The bond-slip behaviour of SFCB–concrete specimens can be predicted by improving the bonding models of FRP bars (Zhao et al., 2020).

In the section above, the bond strength of steel reinforcement bars and tension lap splices of steel bars embedded in concrete were reviewed for NVC and SCC beams. All the test results cited in the literature were on the effect of SCC on bond strength for lap splices of tensile steel reinforcement in regions supporting sagging moments, where the bond conditions were good (see Fig. 1). Very limited studies were cited on top steel in cantilever SCC beams (El Sadany et al. 2020).

3 Research Significance

The bond behaviour of lap splices of tensile steel bars in SCC beams in regions supporting hogging moments (where bond conditions are poor) may exhibit different behavior due to the variable depth of the concrete over the rebars as a result of using non-vibrated self-consolidating concrete. Fig. 1 illustrates the top reinforcement in beams located in poor bond zones given in Eurocode 2 (EN 1992–1–1, 2015). This research will study the effect of SCC on the bond behaviour of the lap splices at poor bond conditions zones typically found as the top reinforcement in cantilevered beams within a zone, where the beam section is subjected to shear and bending. The

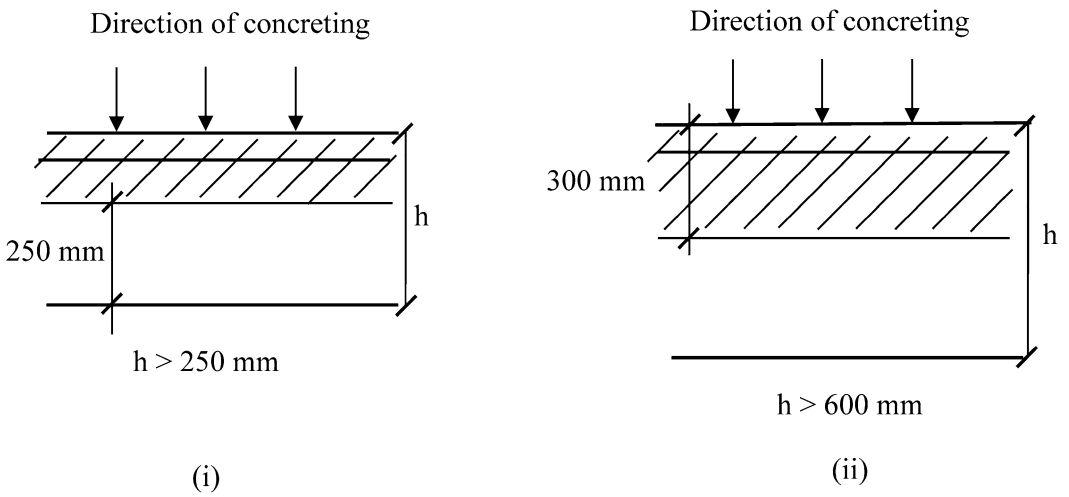

(i) Good bond conditions in the unhatched zone, and (ii) poor bond conditions in the hatched zone.

Fig. 1 Good and poor bond zones according to EC2 (EN 1992–1–1, 2015)

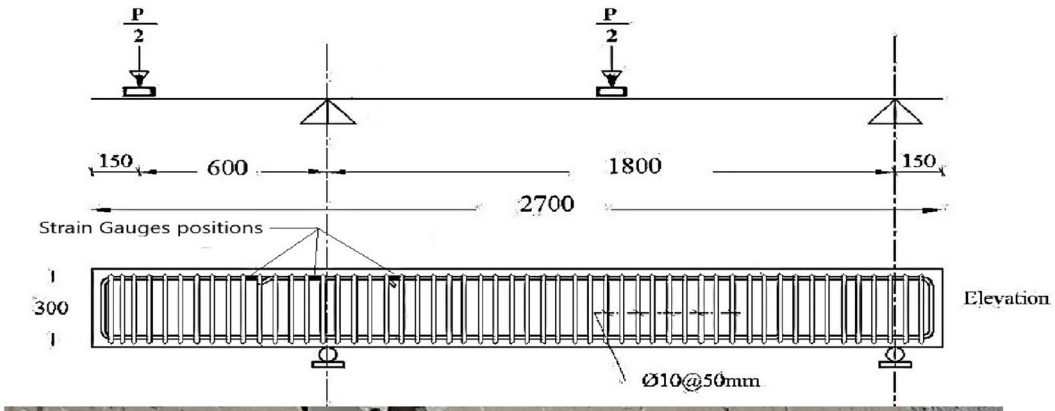

(a)

(b)

(c)

(d)

Fig. 2 **a** Electrical strain gauges' locations, **b** and reinforcement cage, **c** casting a typical beam. **d** Curing of specimens

variables considered include (i) concrete type (SCC and NVC), (ii) characteristic strength (cube concrete compressive strengths at 28 days) of SCC, (iii) lap splice length, and (iv) depth of concrete cover measured from the c.g of the bar to top concrete surface.

4 Experimental Work

This study considered nine simply supported beam specimens that were statically tested under two-point loads. One end was cantilevered, and different reinforcing configurations were detailed, as shown in Figs. 2–4. The objectives of the test program were as follows:

1 Study the rebar bond behaviour during bending failure at the maximum negative (hogging) moment occurring over the cantilever support.

2 Evaluate lap splice efficiency according to Eurocode2 (EN 1992–1–1, 2015) and ECP 203–2018 (Egyptian Code, 2017) using both SCC and NVC.

3 Evaluate the applicability and accuracy of available empirical equations to predict lap splices for SCC beams.

4.1 Test Specimens

The nine beams of rectangular cross-sectional specimens were composed of NVC (used for comparison purposes), normal strength SCC and high-strength SCC. These beams were divided into three groups. The dimensions of beams were: (300 mm deep × 200 mm wide × 2700 mm long). Fig. 2 shows (a) the electrical strain gauges attached to the steel reinforcement in the splice zone, (b) a reinforcement cage and (c) casting of a typical test beam specimen. (d) Curing of specimens using wet burlap. Fig. 3 shows the dimensions and geometry of the test specimens. It can be seen from the figure that only one sample was devoted for the study of concrete cover to focus on the other parameters studied in this research. Table 1 provides the test specimen beam details including groups, mixes, and lap splice length rebar details. It is worth mentioning that the lap splice length was taken as a percentage of anchorage length, L_d, which was measured according to Eurocode2 (EN 1992–1–1, 2015) and ECP 203–2018 (Egyptian Code 2017).

4.2 Materials

The SCC was designed according to EN 206 (BS En 206, 2013) [Concrete. Specification, performance, production, and conformity], considering strength development, density, strength and durability. SCC may exhibit creep or plastic shrinkage more than ordinary concrete mixes because of the high content of limestone powder. As a result, these aspects should be considered when designing SCC. In addition, SCC concrete should be cured as early as possible. SCC workability was within the range of the consistency of SCC described in EN 206 (BS En 206, 2013). Final quantities of one cubic metre of concrete are reported in Table 2. Fresh concrete properties are reported in Table 3.

All steel reinforcement used in this research was high strength deformed steel. Three specimens of each diameter were tested in the lab using Universal Testing Machine, 1000 KN capacity. The average yield stress and ultimate tensile stresses were 586 N/mm^2 and 719 N/mm^2 for the 10 mm diameter bars, and 563 N/mm^2 and 899 N/mm^2 for the 12 mm diameter bars, respectively.

The lap splice length values chosen for this research are 25%, 50% and 100% from the anchorage length obtained from ECP 203–2018 (Egyptian Code 2017) and 27%, 54%, 107% according to Eurocode2 (EN 1992–1–1, 2015). The lap splice length values are reported in Table 1.

4.3 Calculation of the Anchorage Length

The calculation of the anchorage length, l_{bd}, according to Eurocode 2 (EN 1992–1–1, 2015) is

$$l_{bd} = \alpha_1, \alpha_2, \alpha_3, \alpha_4, \alpha_5 l_{b,rqd}\, As_{req}/As_{prov} \quad (1)$$

In addition, the anchorage length values, L_d, were calculated as 68 ϕ for f_{ck} = 28.50 N/mm^2 ($f_{ck,\ cube}$ = 35 N/mm^2) and 46 ϕ for f_{ck} = 53.25 N/mm^2 ($f_{ck,\ cube}$ = 65 N/mm^2).

The calculation of the anchorage Length, L_{d}, according to ECP203-2018 (Egyptian Code 2017) is

$$L_d = \alpha\beta\eta\varphi \frac{(F_y/\gamma_s)}{4f_{bu}} \quad (2)$$

In addition, the anchorage length values, L_{d}, were calculated as 73 ϕ and 56 ϕ for $f_{ck,\ cube}$ = 35 N/mm^2, and 65 N/mm^2, respectively. For example, B6 and B7 have fcu of 65 N/mm2, while the other specimens have fcu of 35 N/mm2. Therefore, the splice lengths of B6 and B7 were different from those of the other specimens.

4.4 Testing Instrumentation

A 400 kN capacity load cell was used to measure the load. Deflections were measured using four dial gauges at the locations shown in Fig. 4. Steel strains across the lap zone were measured using electrical strain gauges. The strain gauges were installed at the beginning (glued to one bar, Location 1), middle (glued to two bars in the splice,

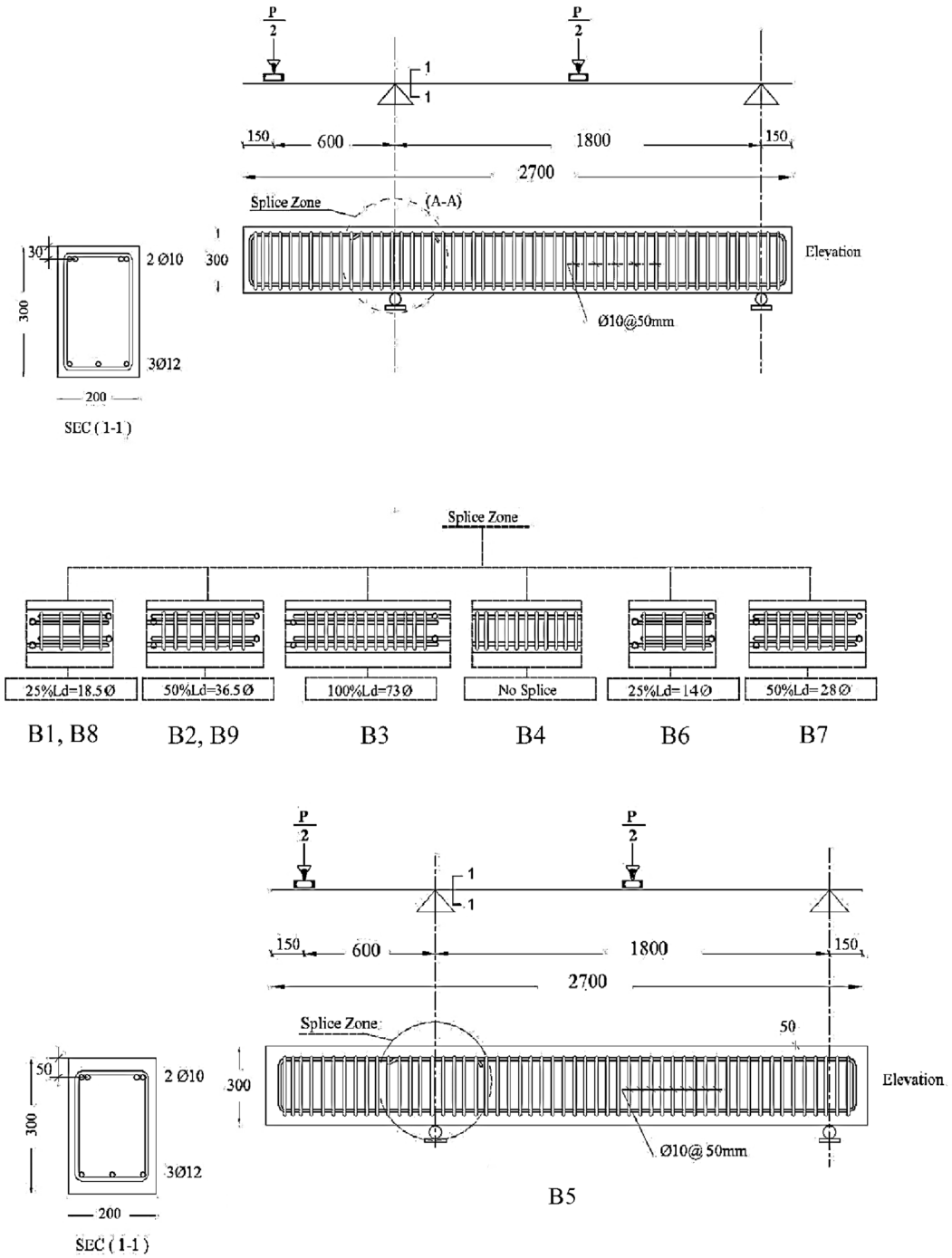

Fig. 3 Geometry and dimensions of studied specimens

Locations 2 and 3) and end of the splice (glued to one bar, Location 4), as shown in Fig. 2. First cracking load and crack width were also measured using demec points, as shown in Fig. 4. It is worth mentioning that the maximum deflection was measured at the location of applied load, end of the cantilever, D.G (1), as shown in Fig. 4, while the strain was measured at the middle, left side and at the right side of the lap splice (four locations, as shown in Fig. 2).

Table 1 Test specimens

Groups	Beam Number	Concrete type	Concrete strength, MPa, $f_{ck,\,cube}$	Concrete Cover, mm	Lap splice length	% of Lap splice length acc. to EC2 (Zhao et al., 2020)	% of Lap splice length acc. to ECP (Sadany et al., 2020)	Top steel rebar	Bottom steel rebar	Stirrup details in tested zone		
										Diameter, mm	Spacing, mm	f_y, N/mm^2
1	B1	SCC	35	30	18.5 ϕ	27% l_{bd}	25% L_d	2 ϕ 10	3 ϕ 12	ϕ 10	50	586
	B2				36.5 ϕ	54% l_{bd}	50% L_d					
	B3				73 ϕ	107% l_{bd}	100% L_d					
	B4				–	No splice	No splice					
	B5			50	18.5 ϕ	27% l_{bd}	25% L_d					
2	B6		65	30	14 ϕ	30% l_{bd}	25% L_d					
	B7				28 ϕ	60% l_{bd}	50% L_d					
3	B8	NVC	35		18.5 ϕ	27% l_{bd}	25% L_d					
	B9				36.5 ϕ	54% l_{bd}	50% L_d					

Table 2 Mixture proportions for SCC1, SCC2 and NVC (kg/m^3)

Materials	* SCC1, $f_{ck,cube}$ = 35 N/mm^2	* SCC2, $f_{ck,cube}$ = 65 N/mm^2	NVC, $f_{ck,cube}$ = 35 N/mm^2
Cement	380	427.5	350
Dolomite (4–15 mm)	616	508	547
Dolomite (15–19 mm)	264	285	650
Sand (0–4)	935	932	753
Mixing water	192.5	153	136.5
Silica fume	–	22.5	–
Limestone powder	112.5	–	–

* For SCC, a high-performance superplasticiser concrete admixture (Viscocrete-3425) was used, whereas a melamine sulfonate polymer-based ordinary water reducer (Sika Control 40) was used in the NVC mixture

4.5 Loading Procedure and Test Setup

The test beams were tested under monotonic loading. They were configured in a four-point bending test, as shown in Fig. 4. Specimens were set over two rigid supports with an 1800 mm simple span and a 600 mm cantilever span. A 300 kN hydraulic actuator was used to apply the load. The load was divided into two concentrated loads separated by a distance of 1500 mm (one at the cantilever free end and the other at the beam midspan) and applied via a rigid steel spreader I-beam. Data from the load cell, extensometer, dial gauges and strain gauges were monitored and recorded.

5 Results and Discussion

5.1 Effect of Splice Lap Length

5.1.1 Crack Pattern

The crack patterns for all test specimens are shown in Fig. 5. For beams B1, B2 and B3, defined in Table 1, the first crack appeared vertically at the ends of lap-splice. These cracks were followed by cracks inside the lap zone, as shown in Fig. 5. With an increase in loading, the horizontal cracks appeared in lap zone parallel to the top reinforcement; the vertical crack extended and started to widen eventually reaching the support. Failure occurred at a maximum moment with formation of vertical cracks in both sides of the beam. For the Beam B4 reinforced with continuous bars without splice, a typical flexural vertical crack first appeared at the top of support in the maximum moment region, followed by cracks appearing vertically in both sides of center line of support.

5.1.2 Cracking and Ultimate Load Capacity

The influence of the lap splice length, L_d on the cracking load was assessed and reported in Table 4. For example, increasing the lap-splice length has increased the first cracking load from 30 kN for B1 to 35 kN for B2 and 40 kN for Beams B3 and B4. In addition, increasing the lap-splice length from 25% L_d to 100% L_d increased the maximum capacity by 36%, as recorded in Table 4.

Although Beam B3 has 100%, L_d, splice length, its ultimate load is less than that of B4 reinforced by continuous steel reinforcement without splice by approximately 13%, as reported in Table 4 and shown in Fig. 6. This may be attributed to the poor bond conditions at the upper steel for SCC.

5.1.3 Load–Deflection Relationships and Energy Absorption

The deflection values under load conditions were measured at the locations indicated in Fig. 4. Load–deflection curves of the Group 1—SCC beams (B1 to B5) are shown in Fig. 6 for the deflections at location at D.G. (1) (see Fig. 4). It can be seen from this figure that the area under load–deflection curves of Beam B3 with splice length (100% L_d) is larger than that of Beam B4 reinforced by continuous steel without splice. It can be argued that the area of main steel reinforcement of B3 is higher than that of B4 with a full development length. Beam B2 of lap splice length, 50% L_d exhibited similar

Table 3 Concrete properties

Test	Units	Mix no.		
		Mix 1	Mix 2	Mix 3
		SCC1	SCC2	NVC
Slump flow (EFNARC-SF2 = 660–750)	mm	700	690	–
Slump flow (T_{500}) (EFNARC-VS1 = 2–5)	s	3.2	3.8	–
J-RING (EFNARC = 0–10) or (< N.M.S)	mm	3	3.4	–
Slump cone (ECP 203–2018 (Code & of Design & Construction of Reinforced Concrete Structures, xxxx) = 75–125)	mm	–	–	100

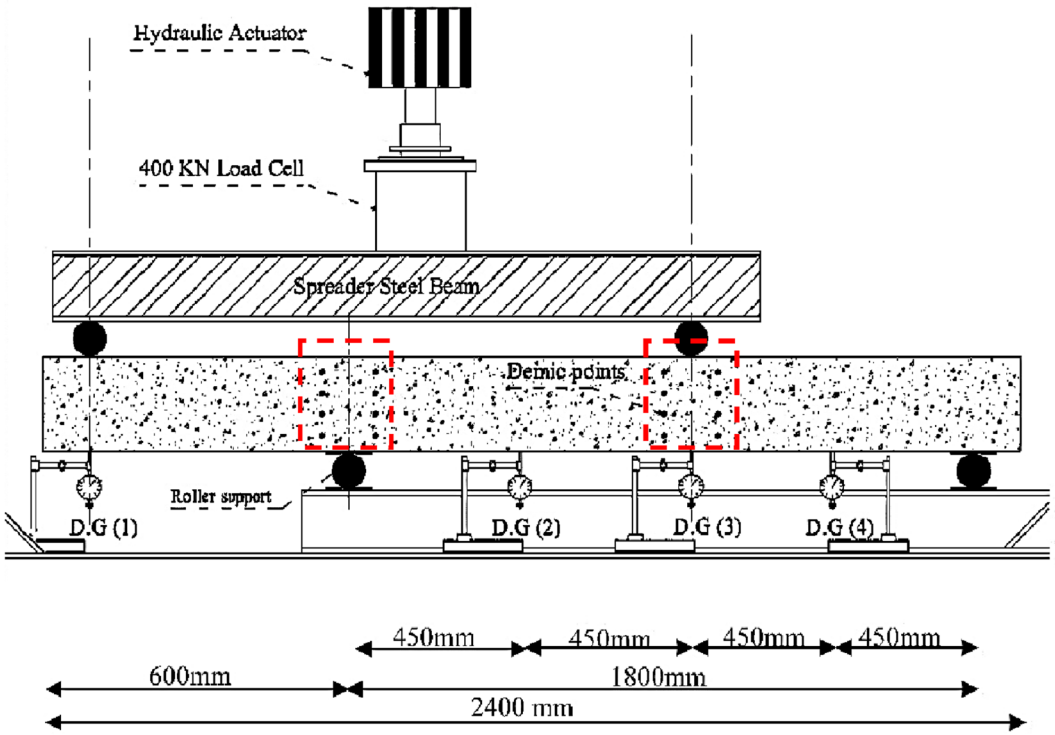

Fig. 4 Test setup

behaviour as that of Beam B3 before cracking but had less moment capacity due to a shorter splice length. Beam B1 of splice length (25% L_d) had the smallest area under the load–deflection curve compared to that of the other beams with same concrete cover in the same group. It is clear from the figure that increasing the lap length allows the beam to behave in a more ductile manner.

Fig. 7 shows that the energy absorption (the area below the load–deflection curve) increased with increasing lap splice length. For example, Beam B3 had an energy absorption of 1144.22 kNmm^2. Also seen from Fig. 7 is that Beam B3 with a lap splice length equals 100% L_d, exhibited energy absorption higher than that of B4 reinforced by continuous steel bars without splices by 28%. This is again could be attributed to the larger area of steel reinforcement of B3 with full development length compared to that of B4.

5.1.4 Bond Stress at the Splice

Bond stress is calculated according to ACI 318 (American Concrete Institute, 2019) and ACI 408R–03 (ACI (American Concrete Institute). 2003) equation:

$$u = \frac{U}{\sum_o} = \frac{\Delta T}{\Delta l \sum_o} = \frac{\Delta f_s A_b}{\Delta l \sum_o} = \frac{\Delta f_s A_b}{4 \Delta l} \tag{3}$$

Bournas et al. (Bournas & Triantafillou, 2011) calculated the bond stress (u) distribution between spliced bars and the surrounding concrete using the following equation:

$$u = \left(\frac{d_b E_S}{4}\right)\left(\frac{\varepsilon_s}{L_d}\right) \tag{4}$$

Bournas et al. (Bournas & Triantafillou, 2011) reported that based on Eq. (4) and by assuming zero strain at the free ends of spliced bars, the bond strength distribution along the splice length, corresponding to peak lateral force, was computed.

Canbay et al. (Canbay & Frosch, 2005) presented the ACI 318 (American Concrete Institute, 2019) equation as follows:

$$\mathrm{U}_u = \frac{f_s d_b}{4 L_d} \tag{5}$$

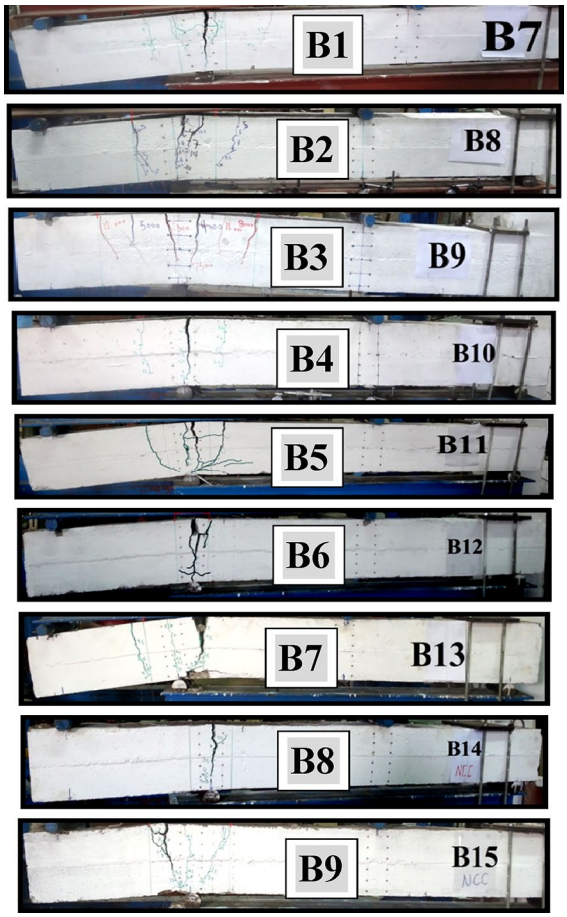

Fig. 5 Crack patterns and failure loads

The stress in the steel, fs, was determined from the maximum load and strain obtained for each beam specimen and was calculated based on elastic cracked section analysis ignoring the tensile stresses in the concrete in tension and considering linear stress–strain behaviour.

The mean bond stress values, *u*, are obtained by direct substitution in Eqs. 4 or 5 and are reported in Table 4. The mean bond stress values for different splice lengths for typical beams are shown in Fig. 8. It can be seen from the figure that Beam B1 (splice length: 25% L_d) had the maximum bond stress. This demonstrates the effect of splice lap length on increasing the bond stress. The bond stress of Beams B2 (splice length: 50% L_d) and B3 (splice length: 100% L_d) were approximately 56% and 30% of that of Beam B1. This may be attributed to the fact that L_d values of Specimens B2 and B3 are two times and four times that of B1.

5.1.5 Ultimate Steel Stress Values Along the Splice-Length

Fig. 9 Shows that the ultimate values of the steel stress calculated along the splice length for a typical 10 mm diameter steel bar in Beams B1, B2 and B3 at different locations of the splice-lengths (see Fig. 2). The figure shows the calculated steel stresses along the splice length for 25% L_d, 50% L_d, and 100% L_d splice length. Increasing the splice length from 25% L_d to 50%, and to 100% L_d led to a rise in the steel stresses by approximately 12% and 20%, respectively. It can be argued that the moment in the upper steel in the shear zone is not constant and this may affect the stresses at the ends of the lap splices which may vary with the change of the lap length.

5.1.6 Load–Steel Strain Relationships

The load strain relationships for longitudinal bars at splices in Specimens B1, B2, B3 and B4 are shown in Fig. 10. It can be seen from the figure that the strain values did not exceed the yield value for high grade steel ($\varepsilon y = 586$ N/mm^2/203000 N/mm^2 = 2887 μstrain) in beams B1 and B2. The recorded steel strains were similar for the beams indicated prior to cracking load, and after cracking until failure. The steel strain decreased with increasing splice length at the same load. This may be attributed to the reduction of stresses in steel bars at the splices as a result of increasing the splice-lengths.

5.2 Effect of Concrete Cover

5.2.1 Crack Pattern

Fig. 5 Shows that increasing concrete cover led to increasing the widths of the cracks. It can be seen that Beam B5 with 50 mm concrete cover had more and larger cracks compared to those of Beam B1 with concrete cover of 30 mm. This may be attributed to the fact that the thicker cover lowered the bars. This reduced the effective depth for the same curvature.

5.2.2 Cracking and Ultimate Load Capacity

Table 4 indicates that increasing concrete cover from 30 mm for B1 to 50 mm for B5, resulted in a reduction in the maximum capacity of B5 by 41%. In addition, increasing the concrete cover to 50 mm for B5, led to a reduction of the first cracking load from 30 to 20 kN, respectively. This may be attributed to the reduction of the effective depth in the section.

5.2.3 Load–Deflection Curve and Energy Absorption

Fig. 6 Shows that the area below the load–deflection curve of Beam B5 with 50 mm concrete cover was approximately 30% of that of Beam B1 having 30 mm concrete cover. This indicates that Specimen B5 failed in a more brittle manner compared to that of B1. In addition, it can be seen from Fig. 7 that Specimen B5

Table 4 Results of the tested beams

Groups	(1)					(2)		(3)	
Beam Number	**B1**	**B2**	**B3**	**B4**	**B5**	**B6**	**B7**	**B8**	**B9**
Bar diameter (mm)	10					10		10	
Type	SCC					SCC		NVC	
$f_{ck,\,cube}$ (N/mm^2)	35					65		35	
Cover (mm)	30				50	30		30	
Lap splice length as percentage of anchorage length according to ECP 203-2018 Code & of Design & Construction of Reinforced Concrete Structures, xxxx	25% L_d	50% L_d	100% L_d	No splice	25% L_d	25% L_d	50% L_d	25% L_d	50% L_d
Lap splice length (mm)	185	365	730	–	185	140	280	185	365
Confinement	ϕ 10@50 mm								
Cracking load, P, kN	30	35	40	40	20	40	45	30	35
Ultimate load, P, kN	110	125	150	172	65	135	160	80	115
Maximum deflection, Δ_{max}, mm, at D.G (1) (see Fig. 4)	4.00	5.40	9.20	7	2.10	5.80	6.70	4.00	5.41
Ultimate strains, ε_{ult} (10^{-3}) at Location 1 (see Fig. 2), E = 203,000 N/mm^2	2.44	2.72	2.93	2.93	2.11	2.93	2.93	2.13	2.45
f_{ult}, N/mm^2, calculated from the maximum load at ultimate strains, ε_{ult}, at Location 1, (see Figs. 2, 9, 11, 17, 23)	495	552	595	–	428	595	595	432	497
u, Mean bond stress, N/mm^2, (ACI-318) (American Concrete Institute, 2019)	6.70	3.78	2.04	–	5.78	10.60	5.31	5.84	3.40
Failure mode	Bond			Flexure	Bond	Bond		Bond	

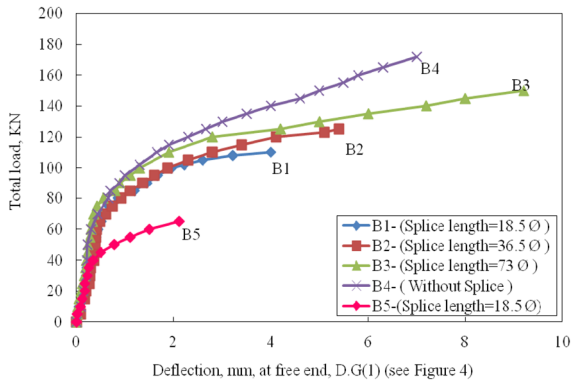

Fig. 6 Load–deflection curves for Group 1 (B1, B2, B3, B4, and B5)

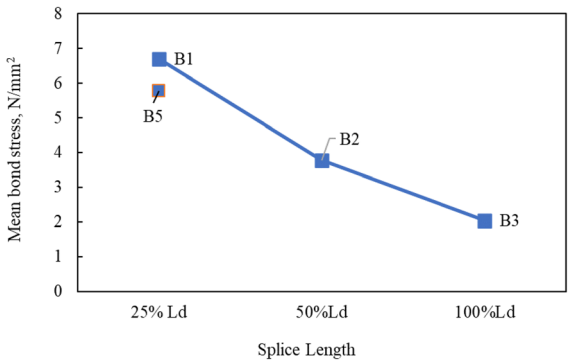

Fig. 8 Bond stress for Beams B1, B2, B3, and B5 (at strain location 1, see Fig. 2)

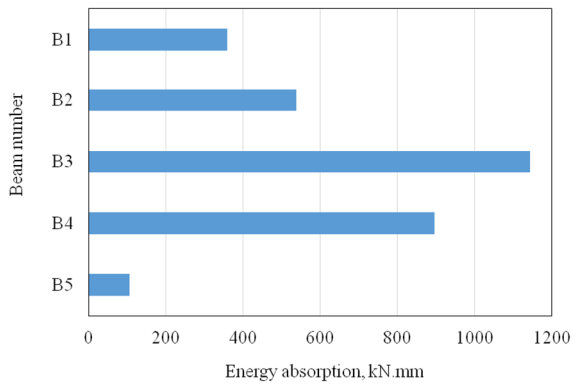

Fig. 7 Energy absorption for Group 1

had a reduction of energy absorption by approximately 71% compared to that of B1. This could be attributed to the fact that the effective depth of B5 was less than that of B1 as a result of increasing the concrete cover and keeping the total thickness constant.

5.2.4 Bond Stress at the Splice

Fig. 8 Shows the bond stresses of Beams B1, B2, B3, and B5. As was stated in Sect. 5.1.4, the bond stress reduces with the increase of the splice length. In addition, although B1 has the same splice length as B5, bond stress in Beam B1 was higher than that of Beam B5 by 16%. This was because the increase in concrete

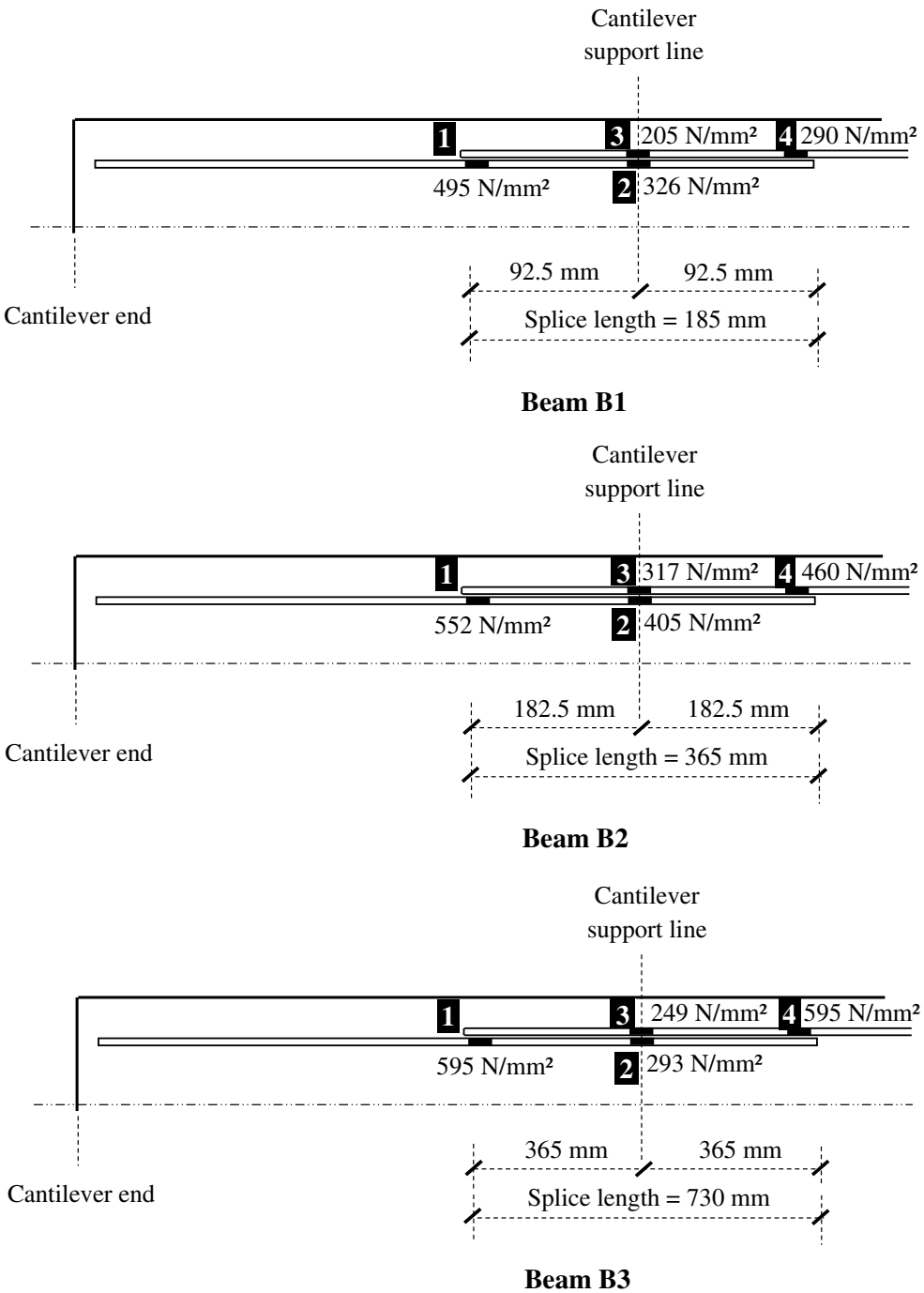

Fig. 9 Ultimate steel stress values calculated from steel strains at strain gauges' locations. Values over 586 N/mm^2 indicate yielding. (Shear links omitted for clarity) Not to scale

cover while keeping the whole thickness of the beam constant in B5 resulted in a reduction of the effective depth, and consequently, the reduction of bond stress in its lap splices.

5.2.5 Ultimate Steel Stress Values Along the Splice Length

Fig. 11 Shows the steel stress values of a steel reinforcement bar of 10 mm diameter for Beam B5. The

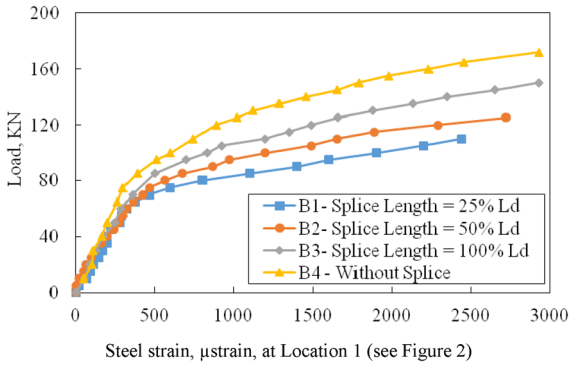

Fig. 10 Load–longitudinal steel strain of Beams B1, B2, B3 and B4

maximum stress at the left side of the lap-splice length was 428 N/mm^2 and reduces toward the right side of the lap-splice length. It can be seen from the figure that the maximum steel stress in Specimen B5 is less than that of Specimen B1 of the same Ld (see Fig. 9) by approximately 16%. This may be attributed again to what was explained above in Sect. 5.2.4 for the reduction of effective depth of Specimen B5.

5.2.6 Load–Steel Strain Curves

The load–strain relationships for the longitudinal bars at splice locations in specimens B1 and B5 are shown in Fig. 12. It can be seen from the figure that the strain values were all less than the yield value for steel reinforcement (2887 µstrain). The recorded steel strains for Specimen B5 are less than those of Specimen B1. This reduction may be attributed to the change in effective depth of the total section as a result of increasing the concrete cover for Beam B5.

5.3 Effect of the Concrete Compressive Strength

5.3.1 Crack Pattern

The effect of compressive strength is shown in Fig. 5 for Group 2—SCC specimens (B6 and B7). Table 1 shows these as having a compressive strength 65 N/mm^2. Fig. 5 shows the flexural crack pattern for B6. The first crack developed in the vertical direction starting from the middle of lap length. This was followed by cracks inside the lap zone. With increasing load, the cracks were concentrated and widened at the middle of the lap splice only and extended to the support. Failure occurred at the maximum moment with the formation of vertical crack on both sides of the beam. Fig. 5 also shows that Beam B7 had a typical first flexural crack pattern, where the cracks concentrated at lap splice ends only. These were followed by cracks inside the lap zone and diagonal cracks near the support following increasing the load. Failure occurred with crushing at the bottom cover at support. It can be observed from the figure that Specimens B6 and B7 behave in a more brittle manner compared to Specimens

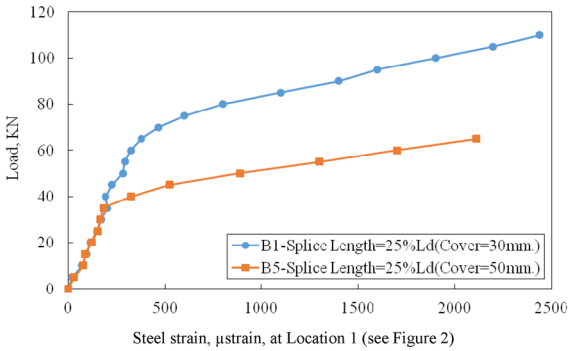

Fig. 12 Load–longitudinal steel strain of Beams B1and B5

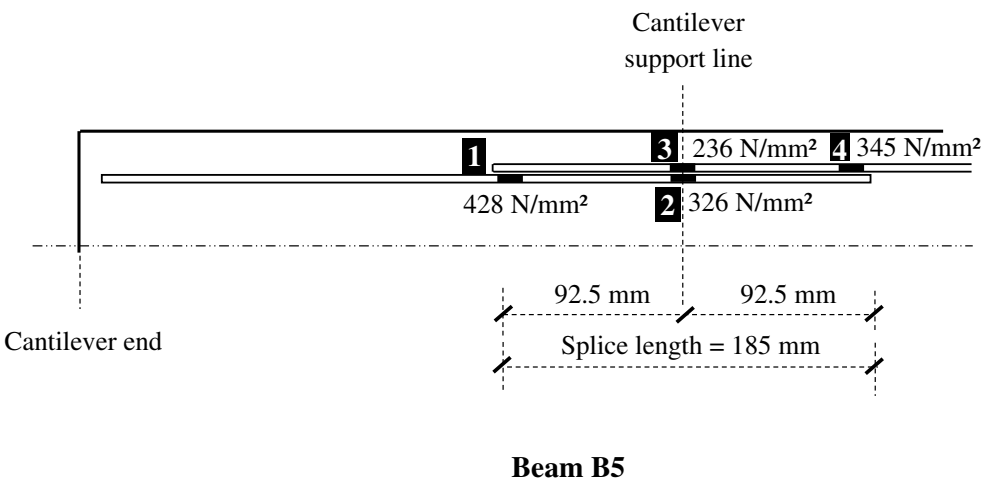

Fig. 11 Ultimate steel stress values calculated from steel strains at strain gauges' locations shown in Fig. 2 (Shear links omitted for clarity) Not to scale

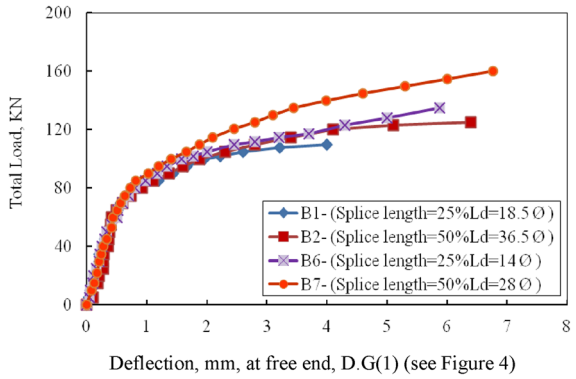

Fig. 13 Load–deflection curves for Beams B1, B2, B6 and B7

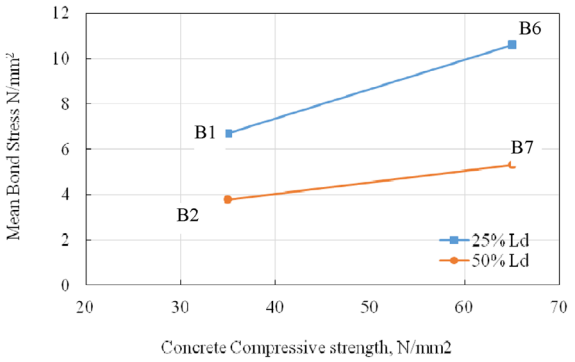

Fig. 15 Bond stress for beams B1, B2, B6 and B7

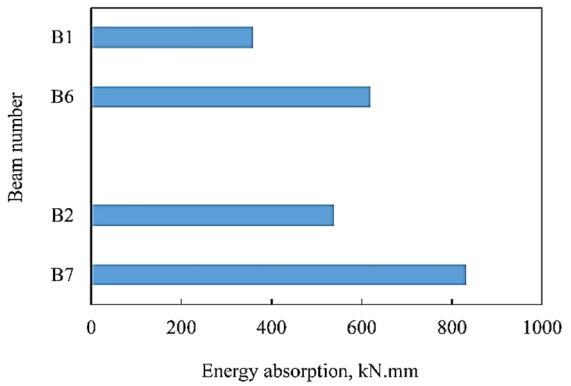

Fig. 14 Energy absorption for beams B1, B2, B6 and B7

B1 to B. It can be argued that the SCC of specimens B6 and B7 had higher strength ($f_{ck,\ cube}$ = 65 N/mm^2) compared to that of the other test specimens which they had normal strength SCC ($f_{ck,\ cube}$ = 35 N/mm^2).

5.3.2 Cracking and Ultimate Load Capacity

From the recorded results in Table 4, increasing splice lap length in Group 2 Beams (B6 and B7) led to an increase in the first cracking load. The first crack appeared at a load of 40 kN for Beam B6 and 45 kN for Beam B7. It can be observed also from Table 4 also that increasing the length of lap-splice from 25% L_d for B6 to 50% L_d for B7 resulted in an increase in the max capacity by 19%. Furthermore, increasing the SCC compressive strength from 35 N/mm^2 for Group 1—SCC specimens B1 and B2, to 65 N/mm^2 for Group 2—SCC specimens B6 and B7, led to an increase in the maximum capacity by an average of 25%.

5.3.3 Load–Deflection Curve and Energy Absorption

Fig. 13 Shows load–deflection curves for beams B1, B2, B6, and B7. It can be seen from the figure that the area under the curve for Beam B1 was approximately 58% of that of Beam B6. This indicates that the ductility of Beam B1 was less than Beam B6. It can also be seen that the area under the curve for Beam B2 was approximately 65% of that of Beam B7. This also indicates that the ductility of Beam B2 was less than that of Beam B7. In addition, energy absorption for Group 2 SCC specimens (B6 and B7) and B1 and B2 from Group 1 SCC beams are shown in Fig. 14. It can be seen from the figure that B6 and B7 with concrete compressive strength, $f_{ck\ cube}$ = 65 N/mm^2 had energy absorptions higher than those of beams with SCC compressive strength, $f_{ck,\ cube}$ = 35 N/mm^2, B1 and B2 by 73% and 54%, respectively. This reduction in ductility for these beams may be attributed to the lower ultimate load as a result of using concrete with lower compressive strength.

5.3.4 Bond Stress at the Splice

The bond stress results for Beams B1, B2, B6, and B7 are shown in Fig. 15. The mean bond stress values of Beams B1 and B2 were approximately 63% and 71% of those of Beams B6 and B7. This may be attributed to the lower concrete strength of Beams B1 and B2 compared to that of Beams B6, and B7.

5.3.5 Ultimate Steel Stress Values Along the Splice Length

Fig. 16 Shows steel stress values along the splice length for Beams B6 and B7. It can be seen from the figure that the maximum steel stress at the left side of the splice length for B6 with 25% L_d and B7 with 50% L_d was the same and equals 595 N/mm^2 which is slightly higher than the yield stress. This may be attributed to the high strength SCC for these specimens which resulted in a better bond for Ld = 25% compared with that of normal strength SCC of the other test specimens. In addition, the non-constant moment in the shear zone would affect the stress at the ends of the lap splices and this may vary with

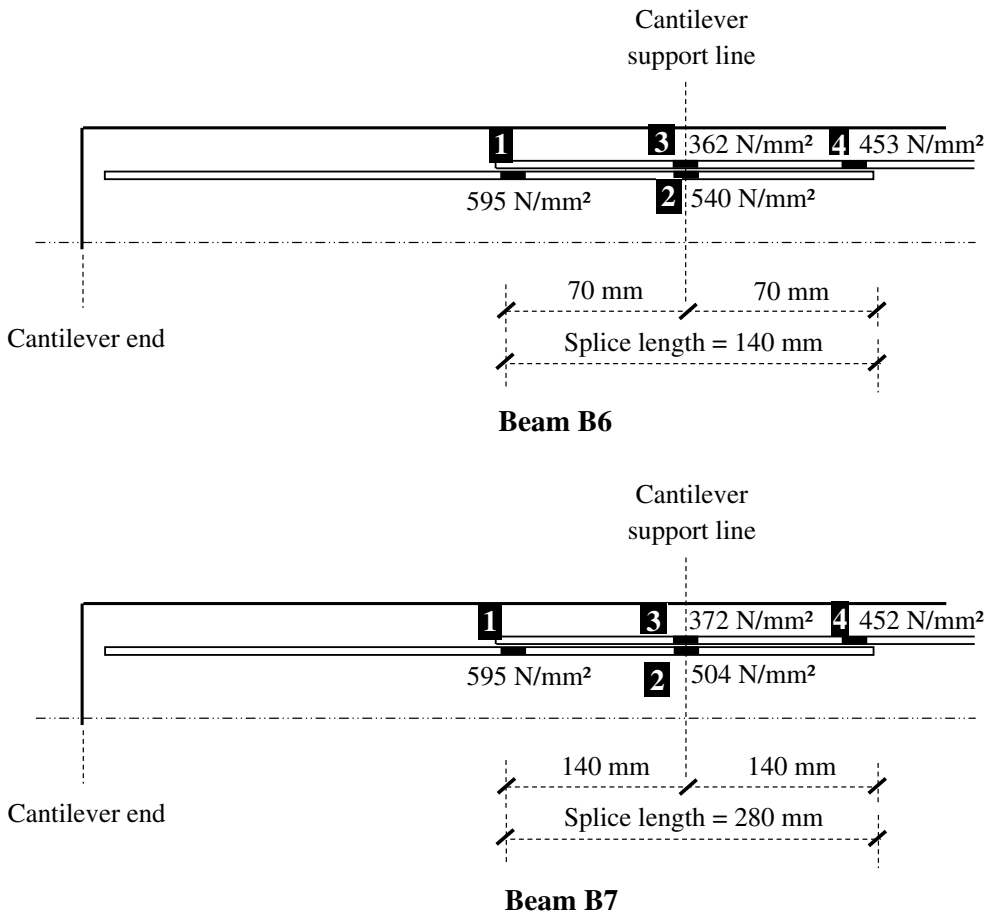

Fig. 16 Ultimate steel stress values calculated from steel strains at strain gauges' locations shown in Fig. 2 (Shear links omitted for clarity) Not to scale

the change of the lap length. Again, the reliability of the results comes from the simulation of the experimental work with what is normally done in the real construction.

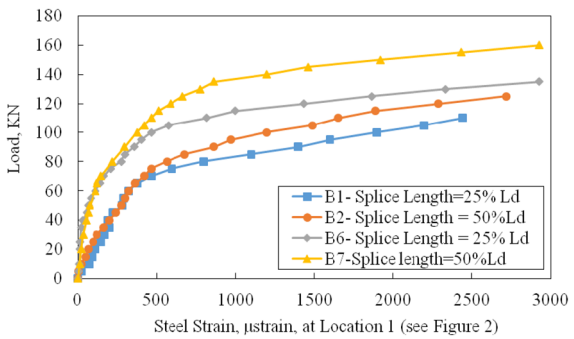

Fig. 17 Load–longitudinal steel strain of Beams B1, B2, B6 and B7

5.3.6 Load–Steel Strain Curve

The load strain relationships for longitudinal bars at splice locations in specimens B1, B2, B6 and B7 are shown in Fig. 17. It can be seen from the figure that the strains did not exceed the yield value for the used steel reinforcement (2887 µstrain) at strain gauge positions 2, 3 and 4. The recorded steel strains show that steel strain of B6 and B7 ($f_{ck,\ cube}$ = 65 N/mm^2) is less than the steel strain of B1 and B2 ($f_{ck,\ cube}$ = 35 N/mm^2) at the same load level. This may be attributed to the increase of concrete compressive strength.

5.4 Effect of Concrete Type (NVC Versus SCC)

5.4.1 Crack Pattern

Crack patterns for Group 3—NVC beams (B8 and B9) are shown in Fig. 5. It can be seen from the figure that Beam B8 had the cracks concentrated at the middle of lap

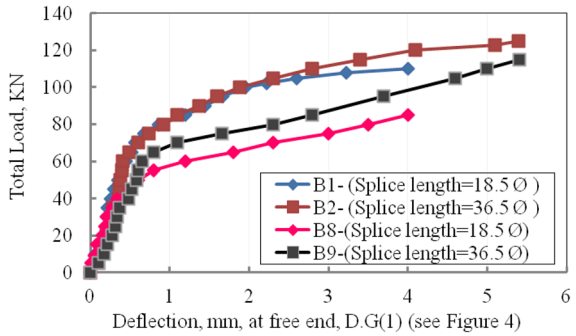

Fig. 18 Load–deflection curves for B1, B2, B8 and B9

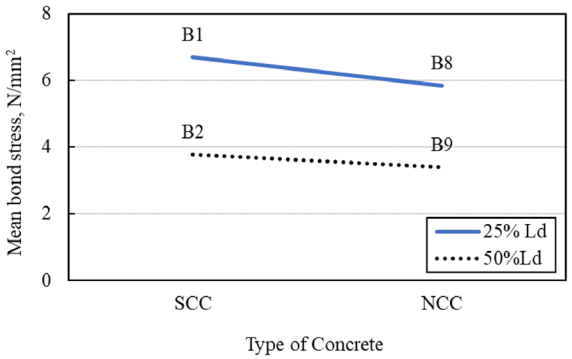

Fig. 20 Bond stress along the lap splice of beams B1, B2, B8 and B9

splice only, getting wider toward the top and reaching the support. Failure occurred at maximum moment with the formation of vertical cracks in both sides of the beams at the end of splice. Beam B9 had the cracks concentrated at lap splice ends only followed by cracks inside the lap zone and diagonal cracks near the support. Failure occurred at maximum moment by formation of vertical crack in both sides of the beam at the end of splice.

5.4.2 Cracking and Ultimate Load Capacity

The first crack appeared at a load of 30 kN for Beam B8, and at 35 kN for Beam B9. Increasing the lap splice length from 25% L_d for B8 to 50% L_d for B9 increased the max capacity by 44%, as reported in Table 4. Comparing B1–B2 with B8–B9, it was found that SCC and NVC beams have the same values of first cracking loads, but the ultimate load for SCC beams increased by 38% for splice length 25% L_d (B1 compared with B8) and approximately 9% for splice length 50% L_d (B2 compared with B9). It can be argued that the bond failure often results from the failure of the concrete which fully encapsulate the bar during placing or bleeding and segregation of the NVC before hardening which reduce the contact on the surface, while the fluidity and cohesion of SCC minimize these negative effects.

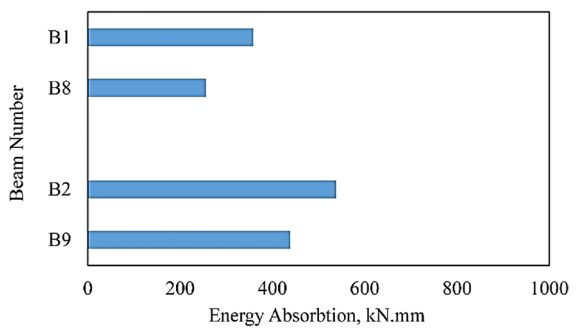

Fig. 19 Energy absorption for beams B1, B2, B8, and B9

5.4.3 Load–Deflection Curve and Energy Absorption

Fig. 18 Shows load–deflection curves for beams in Group 1—SCC (B1–B2) and Group 3—NVC (B8–B9). It can be seen that for Beam B8, the area under the curve was approximately 71% of that of Beam B1. In addition, for Beam B9, the area under the curve was approximately 82% of that of Beam B2. This indicates that the ductility of B8 and B9 is less than those of Beams B1 and B2 due to the lower ultimate loads of B8 and B9. In addition, the figure shows that Beams B1 and B2 exhibited less deflection compared to those of Beams B8 and B9 at the same load level. Fig. 19 shows the energy absorption values of Groups 1—SCC Beams (B1 and B2) and 3—NVC (B8 and B9). It can be seen that the energy absorption values of NVC Specimens B8 and B9 were less than those of SCC Beams B1and B2 by 29% and 18%, respectively. This indicates that SCC enabled the beams to be more ductile and, in turn, resulted in moment capacity improvement for Beams B1 and B2.

5.4.4 Bond Stress at the Splice

The bond stress results for beams B1, B2, B8, and B9 are shown in Fig. 20. The mean bond stress of Beams B1 and B2 are higher than those of B8 and B9 by 15% and 11%, respectively. This indicated that using SCC increased the bond stress in reinforcement bars at splices compared to that of NVC. These findings are generally in agreement with Chan et al. (Chan et al., 2003), Pandurangan et al. (2010) and Turk et al. (Turk et al., 2008) but to different degrees.

5.4.5 Ultimate Steel Stress Values Along the Splice Length

Fig. 21 Shows the steel stress values along the splice length for Beams B8 and B9. It can be seen from the figure that the maximum steel stress at the left side of the lap-splice of B9 with 50% L_d splice length was 497 N/mm^2 which is higher than that of B8 with 25% L_d splice length at the same location by 15%. It can be argued that

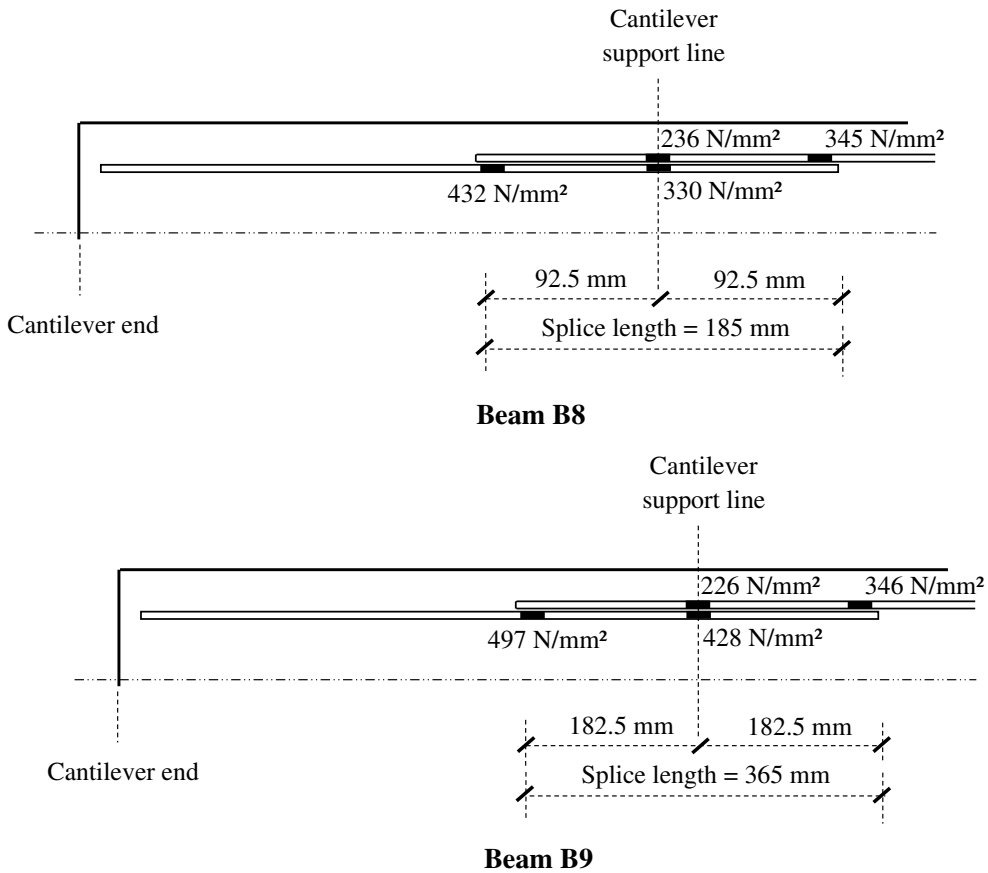

Fig. 21 Ultimate steel stress values calculated from steel strains at strain gauges' locations shown in Fig. 2 (Shear links omitted for clarity) Not to scale

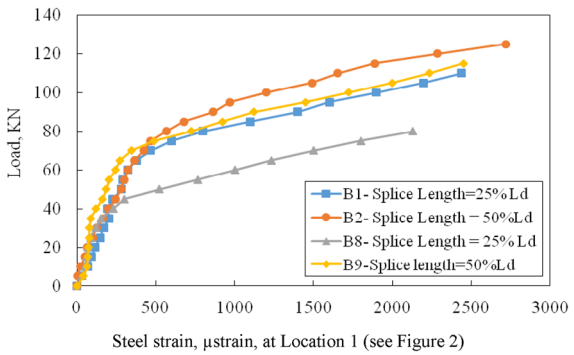

Fig. 22 Load–longitudinal steel strain of Beams B1, B2, B8 and B9

the NVC in these studied specimens behave differently from SCC studied beams. It can be noted for the studied beams that the moment in the shear zone is not constant, and this would affect the stress at the ends of the lap splices and vary with the change of the lap length.

5.4.6 Load–Steel Strain Curves

The load strain relationships for longitudinal bars at the splice locations in specimens B1, B2, B8, and B9 are shown in Fig. 22. It can be seen from the figure that the strains did not exceed the yield strength for the used steel reinforcement (2887 µstrain). The recorded steel strains show that the ultimate steel strain values of Specimens B8 and B9 (NVC) are lower than those of Specimens B1 and B2 (SCC). This may be attributed to the lower ultimate loads of NVC specimens compared to those of SCC counterparts.

6 Prediction of Bond Strength

A number of researchers have developed equations which represent the bond between the reinforcing bars and concrete.

The equation presented by Orangun et al. (Orangun et al., 1977) is expressed as follows:

Table 5 Experimental and predicted bond stress for Beams B1, B2, B6, B7, B8, and B9

Beam ID	Lap splice length	Mean bond stress, N/mm^2, *u*, (Table 4)	Predicted bond stress, *u*, N/mm^2				* Bond efficiency			
			Orangun et al. model (Orangun et al., 1977)	Chapman & Shah (Chapman & Shah, 1987)	Aslani and Nejadi (Aslani & Nejadi, 2012)	Mousavi et al. (Mousavi et al., 2017)	*u*/p (Orangun et al., 1977)	*u*/p (Chapman & Shah, 1987)	*u*/p (Aslani & Nejadi, 2012)	*u*/p (Mousavi et al., 2017)
B1	25% L_d	6.70	5.45	6.76	9.1	6.33	1.23	1.00	0.74	1.06
B6		10.6	7.99	9.82	13.54	9.21	1.33	1.08	0.78	1.15
B8		5.84	5.45	6.76	8.86	6.33	1.07	0.86	0.66	0.92
B2	50% L_d	3.78	4.82	6.08	8.28	5.72	0.78	0.62	0.46	0.66
B7		5.31	6.84	8.58	12	8.05	0.78	0.62	0.44	0.66
B9		3.40	4.82	6.08	8.2	5.72	0.71	0.56	0.41	0.59

* *u*/p = experimental/predicted bond stress

$$\mathrm{U}_u = \left[1.22 + 3.23\frac{c}{d_b} + 53\frac{d_b}{l_d}\right] \sqrt{f_{ck}}\ \text{psi}\ \left(\text{will be converted to N/mm}^2\right) \quad (6)$$

The equation presented by Chapman and Shah (Chapman & Shah, 1987) is expressed as follows:

$$U_u = \left[3.5 + 3.4\left(\frac{c}{d_b}\right) + 57\left(\frac{d_b}{l_d}\right)\right] \sqrt{f_{ck}}\ \text{psi}\ \left(\text{will be converted to N/mm}^2\right) \quad (7)$$

The equations presented by Aslani and Nejadi (Aslani & Nejadi, 2012) is expressed as follows:

For deformed rebar and SCC

$$U_u = \left(0.672\left(\frac{c}{d_b}\right)^{0.6} + 4.8\left(\frac{d_b}{l_d}\right)\right)(f_{ck})^{0.55} \quad (8)$$

For deformed rebar and NVC

$$U_u = \left(0.679\left(\frac{c}{d_b}\right)^{0.6} + 3.88\left(\frac{d_b}{l_d}\right)\right)(f_{ck})^{0.55} \quad (9)$$

The equation presented by Mousavi et al. (Mousavi et al., 2017) is expressed as follows:

$$U_u = \frac{3.9\sqrt{f_{ck}}}{1 + 12e^{-0.54\left(\frac{C_{min}}{d_b} + 10\frac{d_b}{l_d}\right)}} \quad (10)$$

The bond stress values in the current study were calculated according to ACI 318 (American Concrete Institute, 2019), Eqs. (3–5), by substituting the steel stress at ultimate loads. Steel stress values were calculated from first principles using the measured ultimate load strains at Location 1 (see Fig. 2). The calculated bond stress values for the studied beams are reported in Table 4.

The predicted bond stress values using Eqs. (6–10) are recorded in Table 5 and shown in Fig. 23. The bond stress for each specimen was divided by the predicted values to obtain the bond efficiencies listed in Table 5. It can be observed from the table and figure that the predictions obtained by the equations developed by Orangun et al. (Orangun et al., 1977); Chapman and Shah (Chapman & Shah, 1987); Aslani and Nejadi (Aslani & Nejadi, 2012); Mousavi et al. (Mousavi et al., 2017) were in a reasonable agreement with the calculated bond stress values for beams with a splice length equals to 25% L_d. Table 5 shows that the bond efficiencies for Orangun et al. (Orangun et al., 1977) predictions were the best among the four predictions.

On the other hand, Table 5 and Fig. 23 show that the predictions using Eqs. (6–10) overestimated the results for specimens with splice length 50% L_d, In addition, it can be observed that there are discrepancies between the measured bond stress and the values predicted by Eqs. (5–9). It can be argued that the bond stress measured on rather short anchorage lengths is the reliable one, because the true distribution of bond stress is almost uniform and is, therefore, approximated reasonably well by the average bond stress measured. In addition, these equations were originally developed for short splices only.

7 Conclusions

This study investigated the effect of splice lap length, compressive strength, type of concrete (SCC or NVC) and concrete cover depth on the bond behaviour between SCC and top steel bars under tensile loading. The empirical equations given in the design codes (Eurocode2 (EN 1992–1–1, 2015), ECP 203–2018 (Egyptian Code 2017)), for calculating splice lengths for SCC beams were considered. The bond behaviour of lap splices in NVC and SCC were compared, and differences were highlighted as follows.

The increase in splice length from 25% L_d to 100% (full) L_d significantly improved the energy absorption and changed the failure mode of the studied beams to a more ductile manner. The energy absorption of the beam with a splice length of 100% L_d were higher than that of the reference beam by 28%.

The reduction of the effective depth from increasing the concrete cover from 30 to 50 mm, while keeping the total concrete section constant, resulted in a reduction in the maximum ultimate load capacity by 40%, a reduction of the first cracking load by 33%, and a reduction in energy absorption and bond stress by approximately 71%, and 14%, respectively.

The increase in concrete compressive strength from 35 to 65 N/mm^2 increased energy absorption and bond stress by approximately 73%, and 58% for splice length, 25% $L_{d.}$, while the increases were 54%, and 40% for splice length, 50% L_d.

The ultimate load capacity of the SCC specimens with splice lengths of 25% L_d and 50% L_d were higher than that of the NVC specimens by 38% and 9%, respectively. Although no significant difference in ductility was observed, the energy absorption of the NVC specimens were less than that of the SCC specimens by 29% for splice length 25% L_d and by 18% for splice length 50% L_d.

The maximum steel stress in SCC beams in the lap splice zone, was higher than that for NVC specimens. The mean bond stress values, for SCC beams with 25% and 50% lap splice lengths, were higher than those of NVC beams, with the same lap splice lengths, by 15% and

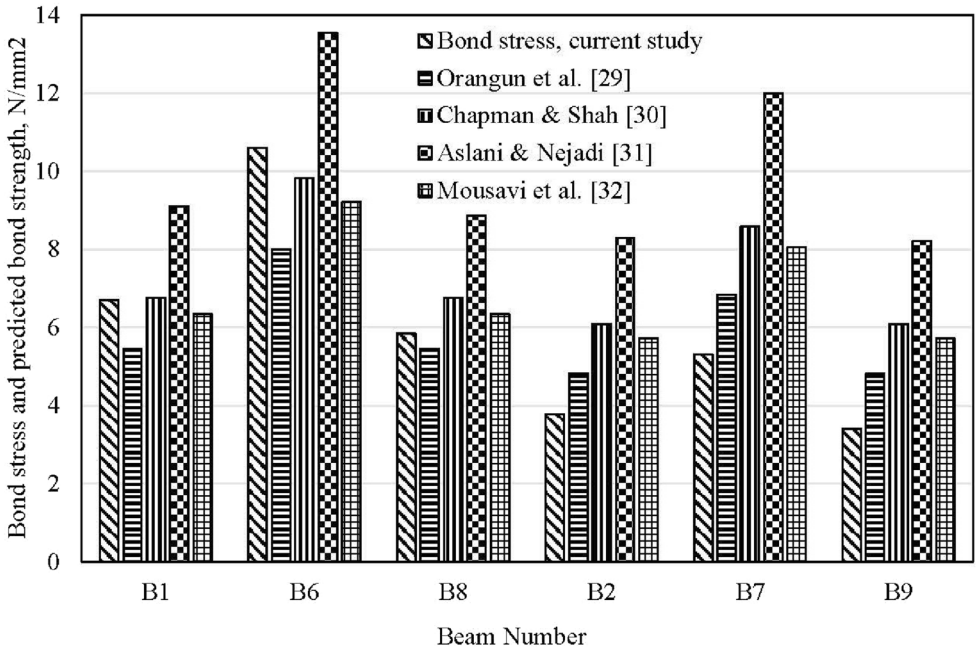

Fig. 23 Bond stress results in the current study and those predicted by other researchers

11%, respectively. The ultimate steel strain of SCC specimens is higher than that of NVC ones.

The empirical equations from the literature were used to predict the bond stress for the studied beams. The prediction was in good agreement with the experimental results for short splice length equals 25% L_d, while it overestimated the results for specimens with longer splices. This agrees with the state of the art as these equations were developed originally for short anchorage lengths.

Abbreviations

As_{req}, As_{prov}	Area of reinforcement required and provided at that section
α	(1–5): Set of coefficients, as given in Table 5.2 (Mosley et al. 1669)
$l_{b,rqd}$	The basic required anchorage length
l_{bd}	The anchorage length (according to EC2 (EN 1992–1–1, 2015)).
L_d	The anchorage length (according to ECP 203-2018 (Egyptian Code 2017)).
σ_{sd}	The maximum value of the design steel stress
α	Straight bars in Tension = 1.0
β	ST. 400/600-in Tension = 0.75
η	Top Reinforcement = 1.3
f_{bd}	: Ultimate bond stress
u	Bond stress
U	Bond force per unit length
$\sum_o$	Sum of the perimeters of the bars developed at a section
A_b	Area of an individual bar or wire
f_s	Tensile stress in reinforcement
E_s	The modulus of elasticity which equals 203,000 N/mm^2
ε_s	The measured steel strains
f_{ult}	Ultimate tensile stress in reinforcement
f_y	Yield stress in steel reinforcement
ε_{ult}	Ultimate strains in steel reinforcement
ε_y	Yield strain in steel reinforcement
U_u	Bond strength of bars
U	Mean bond stress
C	The minimum clear concrete cover
Δ_{max}	Maximum deflection at specific location
d_b	Bar diameter
f_{ck}	The cylinder compressive strength of concrete
$f_{ck,\,cube}$	The cube compressive strength of concrete = 1.2–1.23 f_{ck} [Chapter 3, EC-2 (EN 1992–1–1, 2015)]

Acknowledgements
Not applicable.

Author contributions
Wael Montaser: supervised the student, participated in writing and reviewing it. Ibrahim G. Shaaban: wrote the article, shared in the theoretical work and shared in the final revision. Joseph P. Rizzuto: revised the first draft, shared in the theoretical work and shared in the final revision. Amr H. Zaher: prepared the research plan and shared in the original revision of the paper. Ahmed Rashad (deceased): shared in the research plan and supervised the experimental work. All authors read and approved the final manuscript. All authors read and approved the final manuscript.

Authors' information
Wael Montaser, BSc, MSc, PhD, Associate Professor, Head of Construction and Building Department. Ibrahim G. Shaaban, BSc, MSc, PhD, MICE, CEng, MIStructE, FICE, FIStructE, SFHEA, Reader of Civil Engineering. Joseph P. Rizzuto, BSc, MSc, PhD, CertEd, CEng, MICE, MIStructE, MCIHT, Professor of Civil Engineering. Amr H. Zaher, BSc, MSc, PhD, Professor of Concrete Structures. Ahmed Rashad (deceased), BSc, MSc, PhD, Associate professor. Shorouk Mohamed El Sadany, BSc, MSc, Assistant Lecturer.

Funding
Open access funding provided by The Science, Technology & Innovation Funding Authority (STDF) in cooperation with The Egyptian Knowledge Bank (EKB).

Availability of data and materials
All data generated or analysed during this study are included in this published article.

Competing interests
The authors declare that they have no competing interests. Shorouk Mohamed El Sadany: carried out the experimental work.

Received: 14 July 2022 Accepted: 4 January 2023
Published online: 16 March 2023

References

ACI (American Concrete Institute). (2003). "Bond and development of straight reinforcing bars in tension." ACI 408R–03, Farmington Hills, MI.
Almeida Filho, F. M., Barragán, B. E., Casas, J. R., & El Debs, A. L. H. (2008). Variability of the bond and mechanical properties of self-compacting concrete. *Revista IBRACON De Estruturas e Materiais, 1*(1), 31–57.
American Concrete Institute. (2019). *ACI 318–19 metric building code requirements for structural concrete and commentary*. Farmington Hills: American concrete institute.
Aslani, F., & Nejadi, S. (2012). Bond behavior of reinforcement in conventional and self-compacting concrete. *Advances in Structural Engineering., 15*(12), 2033–2051.
Bournas, D. A., & Triantafillou, T. C. (2011). Bond strength of lap spliced bars in concrete confined with composite jackets. *J Compo Constr.* https://doi.org/10.1061/(ASCE)CC.1943-5614.0000078,156-167
BS EN 206: 2013, Concrete—Specification, performance, production and conformity, British Standards Institution, London, 2013
Canbay, E., & Frosch, R. J. (2005). Bond strength of lap-spliced bars. *ACI Structural Journal, 102*(4), 605–614.
Castel, A., Vidal, T., Viriyametanont, K., & François, R. (2006). Effect of reinforcing bar orientation and location on bond with self-consolidating concrete. *ACI Materials Journal, 103*(4), 559.
Cattaneo, S., & Rosati, G. (2009). Bond between steel and self-consolidating concrete: experiments and modeling. *ACI Structural Journal., 106*(4), 540.
Chan, Y. W., Chen, Y. S., & Liu, Y. S. (2003). Development of bond strength of reinforcement steel in self-consolidating concrete. *Structural Journal, 100*(4), 490–498.
Chapman, R. A., & Shah, S. P. (1987). Early-aged bond strength in reinforced concrete. *ACI Materials Journal., 84*(6), 501–510.
Domone, P. L. (2007). A review of the hardened mechanical properties of self-compacting concrete. *Cement and Concrete Composites, 29*(1), 1–12.
Egyptian Code of Design and Construction of Reinforced Concrete Structures, ECP 203–2018.
El Sadany, S. M., Rashad, A., & Montaser, W. (2020). Bond behavior of upper reinforcing steel bars in self-compacting concrete beams at shear zone. *International Journal of Engineering Research & Technology (IJERT)., 9*(05), 449–458.
El-Azab, M. A., Mohamed, H. M., & Farahat, A. (2014). Effect of tension lap splice on the behavior of high strength self-compacted concrete beams. *Alexandria Engineering Journal., 53*(2), 319–328.
EN 1992–1–1:2015 Eurocode 2—Design of concrete structures—Part 1–1: general rules and rules for buildings.
Esfahani, M. R., Lachemi, M., & Kianoush, M. R. (2008). Top-bar effect of steel bars in self-consolidating concrete (SCC). *Cement and Concrete Composites, 30*(1), 52–60.
Furuya, N., Itohiya, T., & Arima, I. (1994). *Development and application of highly flowing concrete for mass concrete anchorages of Akashi Kaikyo Bridge. Proc of Int Conf on high performance concrete (supplementary papers) Singapore* (pp. 371–396). Detroit, USA: American Concrete Institute.
Khan, S. U., & Ayub, T. (2021). Mechanical properties of hybrid self-compacting fibre-reinforced concrete (SCC-FRC) containing PVA and PP fibres. *Iranian Journal of Science and Technology, Transactions of Civil Engineering.* https://doi.org/10.1007/s40996-021-00652-5
Liu, K., Zou, C., Yan, J., & Shan, X. (2020). Bond behavior of deformed steel bars in self-compacting concrete. *Journal of Adhesion Science and Technology.* https://doi.org/10.1080/01694243.2020.1851937
Miguel, C. S., Nepomuceno, A., & Bernardo, F. L. (2019). Evaluation of self-compacting concrete strength with non-destructive tests for concrete structures. *Applied Science., 9*, 5109. https://doi.org/10.3390/app9235109
Mosley, W. H., Hulse, R., & Bungey, J. H. (1996). *Reinforced concrete design to Eurocode 2 (EC2)*. London: Palgrave Macmillan.
Mousavi, S. S., Dehestani, M., & Mousavi, K. K. (2017). Bond strength and development length of steel bar in unconfined self-consolidating concrete. *Engineering Structures., 131*, 587–598.
Orangun, C. O., Jirsa, J. O., & Breen, J. E. (1977). A reevaluation of test data on development length and splices. *In Journal Proceedings., 74*(3), 114–122.
Pandurangan, K., Kothandaraman, S., & Sreedaran, D. (2010). A study on the bond strength of tension lap splices in self compacting concrete. *Materials and Structures, 43*, 1113–1121. https://doi.org/10.1617/s11527-009-9570-3
Ponmalar, S. (2018). Bond behavior of self-compacting concrete. *Selected Scientific Papers-Journal of Civil Engineering., 13*(s1), 95–105.
Schiessl, A., Zilch, K. (2001) The effect of the modified composition of SCC on shear and bond behavior. In *Proceedings of the 2nd International Symposium on Self-Compacting Concrete, Tokyo, Japan.* 2325, 501506
Self-Compacting Concrete European Project Group, (2005). *The European guidelines for self-compacting concrete: Specification, production and use.* International Bureau for Precast Concrete (BIBM).
Turk, K., Benli, A., & Calayir, Y. (2008). Bond strength of tension lap-splices in full scale self-compacting concrete beams. *Turkish Journal of Engineering and Environmental Science., 32*, 377–386.
Wu, C. H., Chen, M. Y., & Chen, H. J. (2018). Bond behavior of tension bar at lap splice of SCC beam. *Key Engineering Materials, 789*, 126–130. https://doi.org/10.4028/www.scientific.net/KEM.789.126
Zhao, D., Pan, J., Zhou, Y., Sui, L., & Ye, Z. (2020). New types of steel-FRP composite bar with round steel bar inner core: mechanical properties and bonding performances in concrete. *Construction and Building Materials, 242*, 118062. https://doi.org/10.1016/j.conbuildmat.2020.118062
Zhao, D., Zhou, Y., Xing, F., Sui, L., Ye, Z., & Fu, H. (2021). Bond behavior and failure mechanism of fiber-reinforced polymer bar–engineered cementitious composite interface. *Engineering Structures., 243*, 112520. https://doi.org/10.1016/j.engstruct.2021.112520
Zuo, J., & Darwin, D. (2000). Splice strength of conventional and high relative rib area bars in normal and high-strength concrete. *ACI Structural Journal., 97*(4), 630–641.

Publisher's Note

Springer Nature remains neutral with regard to jurisdictional claims in published maps and institutional affiliations.

Submit your manuscript to a SpringerOpen journal and benefit from:

► Convenient online submission
► Rigorous peer review
► Open access: articles freely available online
► High visibility within the field
► Retaining the copyright to your article

Submit your next manuscript at ► springeropen.com